CEAS-GNC-2022-067

CEAS EuroGNC 2022
"Conference on Guidance, Navigation and Control"
3-5 May 2022 @ Technische Universität Berlin, Germany

Incremental Passive Fault-Tolerant Control for Quadrotors With up to Three Successive Rotor Failures

Yannic Beyer PhD Student, TU Braunschweig, Institute of Flight Guidance, 38108, Braunschweig, Germany. y.beyer@tu-braunschweig.de

Fabian Gücker PhD Student, TU Braunschweig, Institute of Flight Guidance, 38108, Braunschweig, Germany. f.guecker@tu-braunschweig.de

Eike Bremers Master's Student, TU Braunschweig, Institute of Flight Guidance, 38108, Braunschweig, Germany. e.bremers@tu-braunschweig.de

Meiko Steen Senior Researcher, TU Braunschweig, Institute of Flight Guidance, 38108, Braunschweig, Germany. m.steen@tu-braunschweig.de

Peter Hecker Professor, TU Braunschweig, Institute of Flight Guidance, 38108, Braunschweig, Germany. p.hecker@tu-braunschweig.de

ABSTRACT

Fault-tolerant control (FTC) can increase the safety of drones, such as quadrotors. It has been known for eight years that the position of quadrotors can still be controlled in case of up to three rotor failures by spinning the quadrotor about an average thrust direction. It has also been shown that the robust incremental nonlinear dynamic inversion (INDI) control concept can be used to transition the quadrotor to the desired state in case a of single rotor failure or two opposing rotor failures. However, the previous concepts use active FTC as they rely on fault detection and isolation. In this paper, up to three rotor failures of quadrotors are investigated using a passive FTC appraoch based on INDI and control allocation. Simulation results show that a single rotor failure or two opposing rotor failures can be compensated but three simultaneous rotor failures lead to a crash. Nevertheless, if the third rotor fails with some time delay, the failure can be compensated since the quadrotor has already started spinning about an average thrust direction before. The results are validated outdoor with a real quadrotor equipped with an inertial measurement unit and a satellite navigation device. Here, it must be ensured that the state estimator remains stable even if the inertial measurement unit spins rapidly and permanently. Furthermore, it can happen with small quadrotors that the occurring rotational speed exceeds the maximum measurable rotational speed of the gyro sensors, which leads to a crash.

Keywords: Quadrotor; Rotor Failure; Incremental Nonlinear Dynamic Inversion; Control Allocation; Passive Fault-Tolerant Control

1 Introduction

Multirotors are widely used for various industrial applications. Quadrotors are a commonly found version of multirotors with four rotors. However, faults like motor or propeller failures (in this paper summarized as rotor failures) of quadrotors can lead to crashes with undesired consequences. Mechanical

Except where otherwise noted, content of this paper is licensed under a Creative Commons Attribution 4.0 International License.

The reproduction and distribution with attribution of the entire paper or of individual pages, in electronic or printed form, including some materials under non-CC-BY 4.0 licenses is hereby granted by the respective copyright owners.

changes to increase flying safety such as increasing the number of rotors or installing parachutes usually bring disadvantages such as lower efficiency. Fault-tolerant control (FTC) is a promising technology for enhancing flying safety because it generally requires only software changes and no mechanical changes. In FTC, a general distinction is made between active and passive FTC. In active FTC, explicit knowledge of the fault is required (through fault detection and isolation) in order to switch the controller mode. In contrast, passive FTC is inherently functional due to high robustness even in the event of a fault. Passive FTC has the advantage over active FTC that no failure can occur due to incorrect fault detection. To date, however, only active fault-tolerant controllers for quadrotor rotor failures have been published. Furthermore, to the best of our knowledge, all fully automatic fault-tolerant controllers for quadrotors have so far only been tested in laboratories or with onboard vision, although the majority of quadrotors are operated outdoors using satellite navigation. In addition, we believe that there is as yet no publication that demonstrates fault-tolerant control that works even in the event of a third rotor failure.

1.1 Previous Work

Standard quadrotor flight controllers usually fail as soon as a rotor fails, but it was shown that quadrotors still can be controlled in the presence of rotor failures by spinning around an average thrust vector [1–3]. Reference [2] has shown that position is still controllable with up to three rotor failures (i.e., with only one rotor intact) when reduced attitude kinematics are used, i.e., when the quadrotor is free to rotate about an axis. The periodic equilibrium with non-zero angular velocity during hover was investigated in Ref. [4] and called *relaxed hover solution*.

In recent years, a number of different flight controllers have been introduced to the scientific community that can still stabilize quadrotors in the event of rotor failures. Different linear controller methods like LQR [2, 5], PID control [6] and linear parameter varying control [7] were investigated. In addition, nonlinear methods such as feedback linearization [1, 3, 8], backstepping [9], incremental nonlinear dynamic inversion (INDI) [10–12] and nonlinear model predictive control [13] were investigated. A nonlinear cascased controller with control allocation (CA) was presented that is able to compensate a complete rotor failure of a quadrotor subjected to large initial rotational rates and arbitrary initial attitude [14].

1.1.1 Passive vs. Active Fault Tolerant Control

None of the previous Refs. [1–14] explicitly use passive FTC. While some references explicitly use or assume active FTC [1, 3, 6, 9, 10], some other references can be assumed to use active FTC based on context [2, 4, 5, 7, 8] or on the provided source code [12]. In the case of the remaining Refs. [11, 14], we cannot, to the best of our knowledge, clearly determine whether the approach is passive or active. Since Ref. [11] seems to be an improvement of Ref. [10] to allow for high-speed flight, we assume that it uses also active FTC. Since Ref. [14] cites a delay typically present before the FTC is triggered as the motivation for the upset recovery problem, we also suspect the use of an active FTC here. Consequently, we believe that there are no publications of passive FTC for quadrotors with complete rotor failures to date. The use of INDI combined with CA for passive FTC control of quadrotors was already discussed in Ref. [15].

1.1.2 Experimental Setup

Numerical simulations with rotor failures are presented in all previously mentioned Refs. [1–14]. The first experimental FTC validation of a quadrotor with one or two opposing rotor failures was published in Ref. [2] using a camera-based external motion capture system. In Refs. [11–14] experimental results with a similar sensor setup are presented. Outdoor experiments were conducted in Ref. [7], however, only an attitude controller was used. A sensor concept with onboard vision was successfully investigated and experimentally validated for the first time in Ref. [8] to compensate for a motor failure. To the best

Except where otherwise noted, content of this paper is licensed under a Creative Commons Attribution 4.0 International License.

The reproduction and distribution with attribution of the entire paper or of individual pages, in electronic or printed form, including some materials under non-CC-BY 4.0 licenses is hereby granted by the respective copyright owners.

of our knowledge, there is no publication yet on FTC of quadrotors subjected to rotor failures validated outdoors with position control using satellite navigation.

1.1.3 Failure Cases

In the previously mentioned publications, different failure cases were investigated such as a single rotor failure [1–4, 6–14], two opposite rotor failures [2, 4–6, 9, 12], and three rotor failures [2, 4]. However, the case of three rotor failures was demonstrated in Refs. [2, 4] only in numerical simulation and without transition from normal operation to the relaxed hover condition. To the best of our knowledge, there is no publication that simulates or experimentally validates the transition from normal operation to compensation for three rotor failures.

1.2 Contributions

We make the following contributions to further increase the safety of quadrotors:

- We present the presumed first passive FTC for quadrotors that is capable of compensating for total rotor failures. The controller is based on INDI and CA. The code is publicly available on Github.[1]
- With the presented passive FTC, we present the presumed first transition from normal operation to the relaxed hover solution in case of three rotor failures. We discuss why a triple rotor failure is a particularly difficult scenario that can only be compensated under specific conditions using the presented passive FTC.
- In flight tests[2], we demonstrate, probably for the first time, rotor-failure compensation of a quadrotor intended for automatic outdoor operation, using an inertial measurement unit and a satellite navigation device.

1.3 Organization

The quadrotor rigid body dynamics and the control task are described in section 2. In section 3 the cascaded control approach with INDI and CA is presented. A small quadrotor with enough power to operate with only one rotor is presented in section 4.1 before the simulation and flight test results are shown in section 4.2 and section 4.3.

2 Problem Formulation

2.1 Notation

We use the conventions of the international standard ISO 1151 in the area of flight dynamics. A lower-case italic subscript of a 3-D vector indicates that the vector is expressed in the corresponding frame. The inertial frame g is represented by the north-east-down coordinate system. The body-fixed frame b is originated at the center of gravity of the vehicle with forward-right-down convention, see Fig. 1a. The upper-case subscript K indicates motion of the body relative to the earth. For symbols that are not part of ISO 1151, we use lower-case boldface symbols to denote vectors, upper-case boldface symbols for matrices and non-boldface symbols for scalars. Normal font subscripts are abbreviations that indicate the affiliation of the symbol: desired (d), filtered (f), reference (ref), control (cntrl), current (0), sensor (sens), motor (mot), battery (bat).

[1]Data available online at `https://github.com/iff-gsc/FTC_Quadrotor_EuroGNC_2022/tree/final_paper_version`. Retrieved April 8, 2022.

[2]Video online at: `https://youtu.be/g6vfgj2IRvE`

Except where otherwise noted, content of this paper is licensed under a Creative Commons Attribution 4.0 International License.

The reproduction and distribution with attribution of the entire paper or of individual pages, in electronic or printed form, including some materials under non-CC-BY 4.0 licenses is hereby granted by the respective copyright owners.

2.2 Quadrotor Flight Dynamics

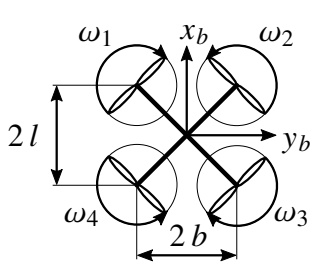

(a) Geometry parameters and rotor definitions.

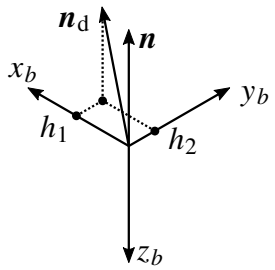

(b) Reduced attitude problem similar to Ref. [12].

Fig. 1 Schematic quadrotor and reduced attitude problem.

2.2.1 Rigid Body Equations of Motion

The six degrees of freedom rigid body equations of motion are applied to compute the angular velocity $\boldsymbol{\Omega}$, the attitude quaternion $\boldsymbol{q}_{bg}$, the velocity $\boldsymbol{V}_K$ and the position $\boldsymbol{s}_g = [\, x \;\; y \;\; z \,]_g^T$ w.r.t. the earth (see Ref. [16], section 1.7):

$$\dot{\boldsymbol{\Omega}}_b = \boldsymbol{I}_b^{-1} \left[\boldsymbol{Q}_b - \boldsymbol{\Omega}_b \times (\boldsymbol{I}_b \boldsymbol{\Omega}_b) \right] , \tag{1}$$

$$\dot{\boldsymbol{V}}_{Kb} = \frac{1}{m} \boldsymbol{R}_b + \boldsymbol{M}_{bg} \begin{bmatrix} 0 & 0 & g \end{bmatrix}^T - \boldsymbol{\Omega}_b \times \boldsymbol{V}_{Kb} , \tag{2}$$

$$\dot{\boldsymbol{q}}_{bg} = \frac{1}{2} \begin{bmatrix} 0 & -p & -q & -r \\ p & 0 & r & -q \\ q & -r & 0 & p \\ r & q & -p & 0 \end{bmatrix} \boldsymbol{q}_{bg} , \tag{3}$$

$$\dot{\boldsymbol{s}}_g = \boldsymbol{M}_{gb} \boldsymbol{V}_{Kb} , \tag{4}$$

with the mass m, the inertia matrix $\boldsymbol{I}$, the force $\boldsymbol{R}$, the moment $\boldsymbol{Q}$, the gravitational acceleration $g = 9.81\,\mathrm{m/s^2}$, $\boldsymbol{\Omega}_b = [\, p \;\; q \;\; r \,]^T$, $\boldsymbol{q}_{bg} = [\, q_0 \;\; q_1 \;\; q_2 \;\; q_3 \,]^T$ and the transformation matrix from inertial g to body frame b $\boldsymbol{M}_{bg} \in \mathrm{SO}(3)$.

2.2.2 Propeller Aerodynamics and Motor Dynamics

For the present application, a simple propeller model can be used to compute the thrust T_i and the drag moment τ_i of the ith propeller (see Fig. 1a) depending on its angular velocity ω_i:

$$T_i = k \cdot \omega_i^2 , \tag{5}$$

$$\tau_i = d \cdot \omega_i^2 . \tag{6}$$

The factors k and d can easily be obtained from publicly available databases, by usage of blade element momentum theory codes or by measurements. Note that this model does not take into account axial or lateral incident flow.

For the brushless motors the direct current motor model of Ref. [17] was applied and validated by measurements:

$$\dot{\omega}_i = -\frac{K_T^2}{R \cdot J} \cdot \omega_i - \frac{\tau_i}{J} + \frac{K_T \cdot V_\mathrm{bat}}{R \cdot J} \cdot u_i , \tag{7}$$

where the angular velocity of the ith motor depends on the drag moment τ_i, battery voltage V_bat, motor duty cycle $0 \leq u_i \leq 1$, motor torque constant K_T, propeller inertia J and motor internal resistance R. In previous work, the motor speed ω_i is used as an input variable to the quadrotor system. However,

Except where otherwise noted, content of this paper is licensed under a Creative Commons Attribution 4.0 International License.

The reproduction and distribution with attribution of the entire paper or of individual pages, in electronic or printed form, including some materials under non-CC-BY 4.0 licenses is hereby granted by the respective copyright owners.

the motor electronic speed controllers (ESCs) for quadrotors in the model building sector typically do not accept a target speed but rather a desired duty cycle u_i from which the speed is an indirect result depending on the motor torque, see Eq. (7). We therefore use the desired duty cycle as an input variable.

2.2.3 Sum of Forces and Moments

The total force vector is the sum of all thrust vectors since other aerodynamic forces are neglected:

$$\boldsymbol{R}_b = \begin{bmatrix} 0 & 0 & -\sum_i T_i \end{bmatrix}^T . \tag{8}$$

The total moment vector

$$\boldsymbol{Q}_b = \underbrace{\begin{bmatrix} b & -b & -b & b \\ l & l & -l & -l \\ 0 & 0 & 0 & 0 \end{bmatrix}}_{\boldsymbol{L}} \boldsymbol{T} + \begin{bmatrix} 0 \\ 0 \\ \sum_i (a_i \tau_i) \end{bmatrix} + \begin{bmatrix} 0 \\ 0 \\ J \sum_i (a_i \dot{\omega}_i) \end{bmatrix} + \begin{bmatrix} Jq(\omega_1 - \omega_2 + \omega_3 - \omega_4) \\ -Jp(\omega_1 - \omega_2 + \omega_3 - \omega_4) \\ 0 \end{bmatrix} - \Gamma \boldsymbol{\Omega}_{Kb} \tag{9}$$

is composed of thrusts times lever arm (see Fig. 1a), propeller drag moments, moments of inertia due to motor acceleration, gyroscopic moments, and rotational damping. The motor rotational direction is defined by $\boldsymbol{a} = [\,-1 \quad 1 \quad -1 \quad 1\,]$. The rotational damping factor $\Gamma > 0$ determines the final angular velocity of the quadrotor after a rotor failure.

2.3 Reduced Attitude Control

Crucial to the success of the FTC is the prioritization and stabilization of the reduced attitude, which is described in Ref. [12]. The task of the attitude controller is to align the measured reduced attitude vector $\boldsymbol{n}$ like the desired reduced attitude vector $\boldsymbol{n}_\mathrm{d}$, see Fig. 1b. For this purpose, the variables h_1 and h_2 are stabilized to zero as in Ref. [12], see Fig. 1b. The desired reduced attitude vector $\boldsymbol{n}_\mathrm{d}$ is specified by the position controller.

3 Control Design

The control concept is based on the control allocation concept of Ref. [15], the reduced attitude concept of Ref. [12] and the idea of incremental position control of Ref. [18] as well as some modifications. The modifications include the different control input definition, use of other control variables for attitude control and different incremental control law for position control. The overall controller consists of two cascades, which are both based on the principle of INDI as shown in Fig. 2. The inner cascade contains the attitude controller, see section 3.2. The outer cascade controls the position, see section 3.4. A crucial part of the presented control concept is the inner loop INDI with CA, which prioritizes the reduced attitude in case of actuator saturations and is presented in section 3.1. For higher performance of the position controller, the outer loop also uses INDI, see section 3.3.

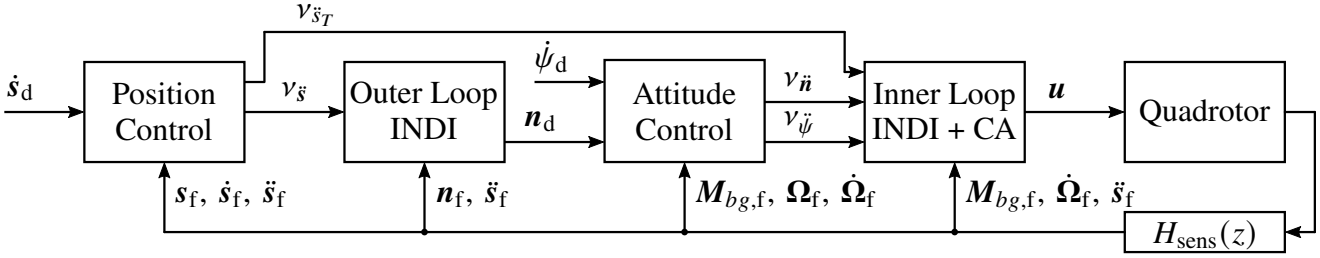

Fig. 2 Block diagram of the overall control system.

Except where otherwise noted, content of this paper is licensed under a Creative Commons Attribution 4.0 International License.

The reproduction and distribution with attribution of the entire paper or of individual pages, in electronic or printed form, including some materials under non-CC-BY 4.0 licenses is hereby granted by the respective copyright owners.

3.1 Inner Loop INDI And CA

The reduced attitude control of Ref. [12] is adopted, which aims to control the direction of the thrust vector $\boldsymbol{n}$ and the quadrotor rotation angle ψ around the unit vector in thrust direction $\boldsymbol{n}$. With this division, rolling and pitching (direction of the thrust vector) can easily be prioritized over the yawing. Additionally, the vertical position is controlled in the inner loop. Therefore, the control variables of the inner loop are

$$\boldsymbol{y} = \begin{bmatrix} h_2 & -h_1 & \psi & z_g \end{bmatrix}^T = \begin{bmatrix} \boldsymbol{C}\,\boldsymbol{n}_{b,\mathrm{d}} & \psi & z_g \end{bmatrix}^T \tag{10}$$

with $\boldsymbol{h} = [\, h_1 \quad h_2 \quad h_3 \,]^T = \boldsymbol{n}_{b,\mathrm{d}} = \boldsymbol{M}_{bg}\,\boldsymbol{n}_{g,\mathrm{d}}$ and $[\, h_2 \quad -h_1 \,]^T = \boldsymbol{C}\,\boldsymbol{n}_{b,\mathrm{d}}$. In order for the controller to handle the upset recovery maneuver, we propose a case distinction in the definition of the control variables as alternative to Eq. (10), but this is not further elaborated in this paper:

$$\boldsymbol{y}_{\mathrm{upset}} = \begin{cases} \begin{bmatrix} h_2 & -h_1 & \psi & z_g \end{bmatrix}^T & \text{if } h_3 < 0\,, \\ \begin{bmatrix} 2\frac{h_2}{\sqrt{h_1^2+h_2^2}} - h_2 & -\left(2\frac{h_1}{\sqrt{h_1^2+h_2^2}} - h_1\right) & \psi & z_g \end{bmatrix}^T & \text{else.} \end{cases} \tag{11}$$

Following the principle of INDI, the control variables are derived until they are statically dependent on the system input. Unlike previous works where commanded motor speeds are defined as system inputs, in this work the motor duty cycles are defined as system inputs, see section 2.2.2. If the motor dynamics is to be neglected as a higher order dynamic for the moment, the steady-state relationship between static duty cycle $\bar{\boldsymbol{u}}$ and static motor speed $\boldsymbol{\omega}$ based on Eq. (7) is required ($\dot{\omega}_i = 0$). For simplicity, we assume that the relationship is linear, i.e., the reduction in motor speed due to applied torque is neglected:

$$\omega_i = \frac{V_{\mathrm{bat}}}{K_T}\bar{u}_i\,. \tag{12}$$

For quadrotors two control effectiveness matrices are considered, one for the motor angular velocity and one for the motor angular acceleration as derived in [19]. Accordingly, in this work, the time derivative of the input variable $\dot{\bar{\boldsymbol{u}}}$ is considered in addition to the static input variable $\bar{\boldsymbol{u}}$. The inner control loop has a relative degree of two, i.e. the second derivative of the control variables depends statically on the static system input $\bar{\boldsymbol{u}}$ and its time derivative $\dot{\bar{\boldsymbol{u}}}$, which can be found be using Eq. (10) and considering Eqs. (1), (2), (8), (9) as well as Eqs. (5) and (6). Now a Taylor series expansion is applied to the second time derivative of Eq. (10) summarizing the current second derivative in $\ddot{\boldsymbol{y}}_0$ and neglecting all derivatives with respect to the system states. Note that this approximation is common for INDI and that it is only valid if the actuator dynamics are significantly faster than the system dynamics:

$$\ddot{\boldsymbol{y}} \approx \ddot{\boldsymbol{y}}_0 + \left.\frac{\partial \ddot{\boldsymbol{y}}}{\partial \bar{\boldsymbol{u}}}\right|_0 \Delta\boldsymbol{u} + \left.\frac{\partial \ddot{\boldsymbol{y}}}{\partial \dot{\bar{\boldsymbol{u}}}}\right|_0 \Delta\dot{\boldsymbol{u}} \approx \begin{bmatrix} \boldsymbol{C}\,\ddot{\boldsymbol{n}}_{b,\mathrm{d},0} \\ \dot{r}_0 \\ \ddot{z}_{g,0} \end{bmatrix} + \frac{\partial}{\partial \bar{\boldsymbol{u}}}\begin{bmatrix} \dot{\boldsymbol{\Omega}} \\ \ddot{z}_g \end{bmatrix}\Bigg|_0 \Delta\boldsymbol{u} + \frac{\partial}{\partial \dot{\bar{\boldsymbol{u}}}}\begin{bmatrix} \dot{\boldsymbol{\Omega}} \\ \ddot{z}_g \end{bmatrix}\Bigg|_0 \Delta\dot{\boldsymbol{u}} \tag{13}$$

with $\ddot{\psi} = \dot{r}$, $\Delta\boldsymbol{u} = \boldsymbol{u} - \bar{\boldsymbol{u}}_0$, $\Delta\dot{\boldsymbol{u}} = \dot{\boldsymbol{u}} - \dot{\bar{\boldsymbol{u}}}_0$, where the subscript 0 indicates the current system state, and

$$\ddot{\boldsymbol{n}}_{b,\mathrm{d}} = \dot{\boldsymbol{\Omega}} \times \boldsymbol{n}_{b,\mathrm{d}} + \boldsymbol{\Omega} \times \dot{\boldsymbol{n}}_{b,\mathrm{d}} + \dot{\boldsymbol{M}}_{bg}\dot{\boldsymbol{n}}_{g,\mathrm{d}} + \boldsymbol{M}_{bg}\ddot{\boldsymbol{n}}_{g,\mathrm{d}}\,. \tag{14}$$

The second approximation in Eq. (13) only holds when $\boldsymbol{n}_{b,\mathrm{d}} \approx [\, 0 \quad 0 \quad -1 \,]^T$. This assumption is made to avoid singularities when $\boldsymbol{n}$ and $\boldsymbol{n}_{\mathrm{d}}$ are perpendicular. This simplification overestimates the control effectiveness for case $|h_3| < 1$.

Except where otherwise noted, content of this paper is licensed under a Creative Commons Attribution 4.0 International License.

The reproduction and distribution with attribution of the entire paper or of individual pages, in electronic or printed form, including some materials under non-CC-BY 4.0 licenses is hereby granted by the respective copyright owners.

Like in previous work [20], a low-pass filter is used to reduce the noise of the sensor signals for $\dot{\boldsymbol{y}}_0$. Typically, the following continuous-time transfer function is selected as filter:

$$H_{\text{sens}}(s) = \frac{1}{\frac{1}{\omega_{\text{sens}}^2}s^2 + \frac{2\zeta_{\text{sens}}}{\omega_{\text{sens}}}s + 1} \tag{15}$$

with natural frequency ω_{sens} and damping ratio ζ_{sens}. These transfer functions are implemented as equivalent discrete-time transfer functions $H_{\text{mot}}(z)$ and $H_{\text{sens}}(z)$. For synchronization all quantities are filtered (subscript f), so that the subscripts 0 in Eq. (14) can be replaced with f [19].

Before solving Eq. (13) for $\Delta\boldsymbol{u}$, we approximate it to discrete-time in z domain with sample time T_{s} by substituting $\Delta\dot{\boldsymbol{u}} = (1 - z^{-1})T_{\text{s}}^{-1}\Delta\boldsymbol{u}$ according to Ref. [19]:

$$\boldsymbol{\nu}_{\dot{\boldsymbol{y}}} \approx \dot{\boldsymbol{y}}_{\text{f}} + \left(\tilde{\boldsymbol{G}}_1 + \frac{1}{T_{\text{s}}}\tilde{\boldsymbol{G}}_2\right)\Delta\boldsymbol{u} - \tilde{\boldsymbol{G}}_2\frac{z^{-1}\Delta\boldsymbol{u}}{T_{\text{s}}}\,, \tag{16}$$

where the predicted acceleration $\dot{\boldsymbol{y}}$ is already replaced by the desired acceleration, the so-called called pseudo-control input $\boldsymbol{\nu}_{\dot{\boldsymbol{y}}}$, with

$$\tilde{\boldsymbol{G}}_1 = \frac{\partial}{\partial\bar{\boldsymbol{u}}}\begin{bmatrix}\dot{\boldsymbol{\Omega}}\\ \ddot{z}_g\end{bmatrix}\Bigg|_{\text{f}} \approx \frac{\partial}{\partial\boldsymbol{\omega}}\begin{bmatrix}\dot{\boldsymbol{\Omega}}\\ \ddot{z}_g\end{bmatrix}\Bigg|_{\text{f}}\frac{\partial\boldsymbol{\omega}}{\partial\bar{\boldsymbol{u}}}\Bigg|_{\text{f}} \approx 2\boldsymbol{I}_b^{-1}\left(k\boldsymbol{L} + d\begin{bmatrix}0 & 0 & 1\end{bmatrix}^T\boldsymbol{a}\right)\bar{\boldsymbol{u}}\left(\frac{V_{\text{bat}}}{K_T}\right)^2 \tag{17}$$

and

$$\tilde{\boldsymbol{G}}_2 = \frac{\partial}{\partial\dot{\bar{\boldsymbol{u}}}}\begin{bmatrix}\dot{\boldsymbol{\Omega}}\\ \ddot{z}_g\end{bmatrix}\Bigg|_{\text{f}} \approx \frac{\partial}{\partial\dot{\boldsymbol{\omega}}}\begin{bmatrix}\dot{\boldsymbol{\Omega}}\\ \ddot{z}_g\end{bmatrix}\Bigg|_{\text{f}}\frac{\partial\boldsymbol{\omega}}{\partial\bar{\boldsymbol{u}}}\Bigg|_{\text{f}} = \boldsymbol{I}_b^{-1}J\begin{bmatrix}0 & 0 & 1\end{bmatrix}^T\boldsymbol{a}\frac{V_{\text{bat}}}{K_T}\,. \tag{18}$$

Equation (16) is subjected to

$$(\boldsymbol{u}_{\min} - \bar{\boldsymbol{u}}_{\text{f}}) \le \Delta\boldsymbol{u} \le (\boldsymbol{u}_{\max} - \bar{\boldsymbol{u}}_{\text{f}}) \quad \text{with } \boldsymbol{u}_{\min} = \boldsymbol{0},\ \boldsymbol{u}_{\max} = \boldsymbol{1} \tag{19}$$

and is solved for $\Delta\boldsymbol{u}$ with the weighted least squares (WLS) CA algorithm of Ref. [15] which is an adaption for incremental control inputs based on Ref. [21] (in the implementation we use QCAT[3]):

$$\Delta\boldsymbol{u} = \underset{\Delta\boldsymbol{u}\in[\boldsymbol{0}-\boldsymbol{u}_0,\,\boldsymbol{1}-\boldsymbol{u}_0]}{\arg\min}\ c(\Delta\boldsymbol{u}) \quad \text{with} \quad c(\Delta\boldsymbol{u}) = \left\|\begin{bmatrix}\gamma^{\frac{1}{2}}\boldsymbol{W}_v\boldsymbol{G}\\ \boldsymbol{W}_u\end{bmatrix}\Delta\boldsymbol{u} - \begin{bmatrix}\gamma^{\frac{1}{2}}\boldsymbol{W}_v\boldsymbol{v}\\ \boldsymbol{W}_u\boldsymbol{u}_{\text{d}}\end{bmatrix}\right\|^2, \tag{20}$$

where the cost function $c(\Delta\boldsymbol{u})$ is a combination of the primary pseudo-control error cost and the secondary input actuation cost with $\boldsymbol{v} = \boldsymbol{\nu}_{\dot{\boldsymbol{y}}} - \dot{\boldsymbol{y}}_{\text{f}} + T_{\text{s}}^{-1}\tilde{\boldsymbol{G}}_2 z^{-1}\Delta\boldsymbol{u}$ and $\boldsymbol{G} = \tilde{\boldsymbol{G}}_1 + T_{\text{s}}^{-1}\tilde{\boldsymbol{G}}_2$. $\boldsymbol{W}_v = \text{diag}(w_{\dot{p}}, w_{\dot{q}}, w_{\dot{r}}, w_{\ddot{z}})$ is the diagonal weighting matrix for the control objective, and $\boldsymbol{W}_u$ is the diagonal weighting matrix for the inputs. The distinction between the primary and secondary objective is made by the scale factor $\gamma \gg 1$.

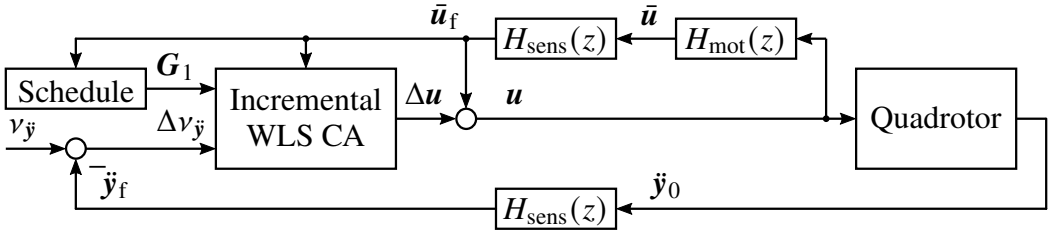

Fig. 3 Block diagram of inner loop INDI and CA.

[3]Ola Harkegard (2022). QCAT (`https://www.mathworks.com/matlabcentral/fileexchange/4609-qcat`), MATLAB Central File Exchange. Retrieved January 20, 2022.

Except where otherwise noted, content of this paper is licensed under a Creative Commons Attribution 4.0 International License.

The reproduction and distribution with attribution of the entire paper or of individual pages, in electronic or printed form, including some materials under non-CC-BY 4.0 licenses is hereby granted by the respective copyright owners.

Figure 3 shows the block diagram of the inner loop INDI and CA. The actuator states can either be obtained from measurement or from a model. In this work they are obtained from a model. Using a model increases the robustness against actuator faults as shown later. A first order transfer function is used as the actuator model, which is obtained by neglecting the propeller drag moment in Eq. (7), with the following Laplace transform:

$$\tilde{H}_{\text{mot}}(s) = \frac{K_{\text{mot}}}{T_{\text{mot}} s + 1} = K_{\text{mot}}\, H_{\text{mot}}(s) \tag{21}$$

with motor time constant $T_{\text{mot}} = RJK_T^{-2}$ and static gain $K_{\text{mot}} = K_T V_{\text{bat}}$.

3.2 Attitude Control

The inner loop pseudo-control input is divided into attitude control and altitude control: $\boldsymbol{\nu}_{\ddot{y}} = [\, \boldsymbol{\nu}_{y_{\text{atti}}} \;\; \nu_{\ddot{z}} \,]^T$. The pseudo-control input of the attitude controller $\boldsymbol{\nu}_{\ddot{y}_{\text{atti}}}$ is composed of the reference model and the feedback gains:

$$\boldsymbol{\nu}_{\ddot{y}_{\text{atti}}} = \boldsymbol{\nu}_{\ddot{\boldsymbol{y}}_{\text{atti}},\text{ref}} + \boldsymbol{\nu}_{\ddot{\boldsymbol{y}}_{\text{atti}},\text{cntrl}} \,. \tag{22}$$

The feedback controller includes three gains $k_{()}$ for each of the three control variables. They can be designed by any linear control design technique considering the ideally inverted system (chain of integrators and delay due to actuator dynamics and sensor filters [19]) in Fig. 4:

$$\boldsymbol{\nu}_{\ddot{\boldsymbol{y}}_{\text{atti}},\text{cntrl}} = \begin{bmatrix} k_n e_{h_2} + k_{\dot{n}} \dot{e}_{h_2} + k_{\ddot{n}} \ddot{e}_{h_2} \\ k_n e_{h_1} + k_{\dot{n}} \dot{e}_{h_1} + k_{\ddot{n}} \ddot{e}_{h_1} \\ k_\psi e_\psi + k_{\dot{\psi}} e_r + k_{\ddot{\psi}} \dot{e}_r \end{bmatrix} , \tag{23}$$

where $e_{()}$ denotes the control error, e.g. $e_{h_2} = h_{2,\text{ref}} - h_{2,\text{f}}$.

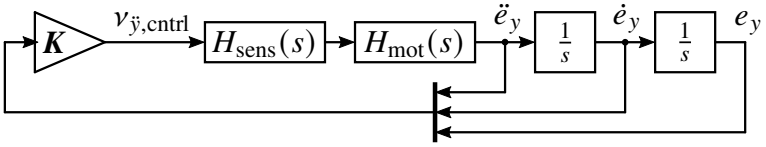

Fig. 4 Block diagram of the attitude error dynamics for the ideally inverted system with $\boldsymbol{K} = [\, k_{\ddot{y}} \; k_{\dot{y}} \; k_y \,]$.

The desired attitude inputs ψ_d and $\boldsymbol{n}_\text{d}$ are filtered by a second order reference model, which outputs the reference signals with first and second time derivatives, see Fig. 5. The second time derivative of the reference signal is part of the pseudo-control input in Eq. (22). For the calculation of the control error, the reference signals are filtered equivalently to the feedback signal, see Fig. 5.

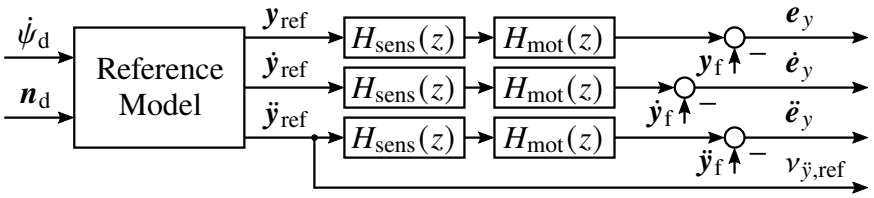

Fig. 5 Attitude controller reference model and control error computation with $\boldsymbol{y} = \boldsymbol{y}_{\text{atti}}$.

3.3 Outer Loop INDI

Using INDI in the outer loop has two advantages over using NDI: The system responds significantly faster to disturbances such as wind gusts and no integrating controller (I controller) is needed to achieve steady-state accuracy [18]. Unlike Ref. [18], in which INDI is based on linearization, in this work the

Except where otherwise noted, content of this paper is licensed under a Creative Commons Attribution 4.0 International License.

The reproduction and distribution with attribution of the entire paper or of individual pages, in electronic or printed form, including some materials under non-CC-BY 4.0 licenses is hereby granted by the respective copyright owners.

control law typically used for NDI [12] is modified to get an equivalent incremental control law for the desired reduced attitude vector:

$$\Delta \boldsymbol{n}_\mathrm{d} = \frac{\boldsymbol{\nu}_{\ddot{s}} - \ddot{\boldsymbol{s}}_\mathrm{f}}{\|\ddot{\boldsymbol{s}}_\mathrm{f} - \boldsymbol{g}\|}\,, \tag{24}$$

$$\boldsymbol{n}_\mathrm{d} = \frac{\boldsymbol{n}_\mathrm{f} + \Delta \boldsymbol{n}_\mathrm{d}}{\|\boldsymbol{n}_\mathrm{f} + \Delta \boldsymbol{n}_\mathrm{d}\|}\,. \tag{25}$$

In contrast to the inner control loop, no model is used for the dynamics of the system input $\boldsymbol{n}$, but the measurement of the reduced attitude $\boldsymbol{n}_\mathrm{f}$. With this controller, the same disturbance transfer function is obtained as in Ref. [18]. In addition, satisfying control performance is obtained even with large deviations between the desired acceleration $\boldsymbol{\nu}_{\ddot{s}}$ and the filtered acceleration $\ddot{\boldsymbol{s}}_\mathrm{f}$. Singularities should be avoided by limiting the denominators of Eqs. (24) and (25) to values greater than zero.

3.4 Position Control

The desired acceleration vector depends on a reference from the reference model $\boldsymbol{\nu}_{\ddot{s},\mathrm{ref}}$ in case of commanded position changes and on a part contributed by the feedback controller $\boldsymbol{\nu}_{\ddot{s},\mathrm{cntrl}}$:

$$\boldsymbol{\nu}_{\ddot{s}} = \boldsymbol{\nu}_{\ddot{s},\mathrm{ref}} + \boldsymbol{\nu}_{\ddot{s},\mathrm{cntrl}}\,. \tag{26}$$

Since no position changes are commanded in this paper, $\boldsymbol{\nu}_{\ddot{s},\mathrm{ref}} = \boldsymbol{0}$. The feedback controller includes three gains $k_{()}$ for each of the three directions that can be designed by any linear control design technique similarly to section 3.2:

$$\boldsymbol{\nu}_{\ddot{s},\mathrm{cntrl}} = \begin{bmatrix} k_s e_x + k_{\dot{s}} \dot{e}_x + k_{\ddot{s}} \ddot{e}_x \\ k_s e_y + k_{\dot{s}} \dot{e}_y + k_{\ddot{s}} \ddot{e}_y \\ k_s e_z + k_{\dot{s}} \dot{e}_z + k_{\ddot{s}} \ddot{e}_z \end{bmatrix}\,. \tag{27}$$

The component in thrust direction $\nu_{\ddot{s}_T}$ is filtered by a low pass filter with the same design as the attitude controller reference model and then passed to the inner loop INDI and CA.

4 Results

The passive fault-tolerant controller is investigated by nonlinear simulation, see section 4.2, and flight tests, see section 4.3. The quadrotor used and the parameters used for the simulation model are presented in section 4.1.

4.1 Presentation of the Used Quadrotor

The flight tests are performed with the custom built quadrotor Minnie, see Fig. 6a. All parameters required for the simulation model, see section 2.2, were measured or estimated and are shown in Tab. 1. The main components are listed in Tab. 3 in the appendix. All controller parameters of the controller presented in section 3 are shown in Tab. 2.

To operate outdoors, the quadrotor is equipped with an inertial measurement unit (IMU), a satellite navigation device (GPS) as well as magnetic sensor. The flight controller board is a Matek H743-SLIM. An IMU of the type MPU6000 and an IMU of the type ICM42605 are integrated on this board for measurement of the angular rate and specific force. Additionally, the GPS and compass module M8Q-5883 is connected. The rigid body state of the quadrotor is estimated using the Extended Kalman Filter (EKF) of ArduPilot version ArduCopter V4.2.0-dev[4]. The implementation consists of a real time inertial navigation system (INS) and an EKF running at a delayed fusion time horizon. The difference between the INS and EKF is then used to correct the INS using a simple error gain. The EKF becomes unstable

[4]Final source code for flight test: `https://github.com/ybeyer/ardupilot/tree/EuroGNC_2022_flight_test`

Except where otherwise noted, content of this paper is licensed under a Creative Commons Attribution 4.0 International License.

The reproduction and distribution with attribution of the entire paper or of individual pages, in electronic or printed form, including some materials under non-CC-BY 4.0 licenses is hereby granted by the respective copyright owners.

(a) Complete quadrotor.

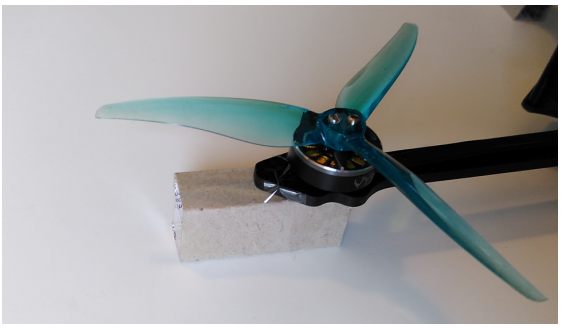

(b) Attached cardboard drag plate in order to increase the yaw damping in flight tests.

Fig. 6 Photos of the custom built quadrotor Minnie with enough power to operate with only one motor.

Table 1 Quadrotor parameters.

Symbol	Value	Unit	Symbol	Value	Unit	Symbol	Value	Unit
m	0.43	kg	I_{xx}	$1.1\,\mathrm{E}-3$	$\mathrm{kg\,m^2}$	K_T	$5.6\,\mathrm{E}-3$	$\mathrm{N\,m/A}$
l	$7.95\,\mathrm{E}-2$	m	I_{yy}	$9.9\,\mathrm{E}-4$	$\mathrm{kg\,m^2}$	R	0.32	Ω
b	$9.90\,\mathrm{E}-2$	m	I_{zz}	$1.8\,\mathrm{E}-3$	$\mathrm{kg\,m^2}$	V_{bat}	22.2	V
k	$1.06\,\mathrm{E}-6$	$\frac{\mathrm{N}}{(\mathrm{rad/s})^2}$	I_{xz}	$-1.6\,\mathrm{E}-5$	$\mathrm{kg\,m^2}$	J	$2.6\,\mathrm{E}-6$	$\mathrm{kg\,m^2}$
d	$9.9\,\mathrm{E}-9$	$\frac{\mathrm{N\,m}}{(\mathrm{rad/s})^2}$	I_{yz}	$2.1\,\mathrm{E}-8$	$\mathrm{kg\,m^2}$	Γ	$1.0\,\mathrm{E}-3$	$\frac{\mathrm{N\,m}}{\mathrm{rad/s}}$

Table 2 Parameters of the flight controller. Note that there are more parameters for the yawing reference model as well as the lateral position reference model but these are not needed in this work.

Symbol	Value	Unit	Symbol	Value	Unit	Symbol	Value	Unit
k_s	3.353	$\mathrm{s^{-2}}$	$w_{\dot{p}}$	10	$\mathrm{s^2/rad}$	ω_{sens}	503	rad/s
$k_{\dot{s}}$	3.901	$\mathrm{s^{-1}}$	$w_{\dot{q}}$	10	$\mathrm{s^2/rad}$	ζ_{sens}	1	–
$k_{\ddot{s}}$	0.7114	–	$w_{\dot{r}}$	0.01	$\mathrm{s^2/rad}$	ω_n	15	rad/s
k_n	200	$\mathrm{s^{-2}}$	$w_{\ddot{z}}$	1	$\mathrm{s^2/m}$	ζ_n	1	–
$k_{\dot{n}}$	39.96	$\mathrm{s^{-1}}$	w_{u_i}	1	–	T_{s}	$2.5\,\mathrm{E}-3$	s
$k_{\ddot{n}}$	0.9513	–	γ	1000	–			
k_ψ	50	$\mathrm{s^{-2}}$	u_{d}	0.1	–			
$k_{\dot{\psi}}$	15.61	$\mathrm{s^{-1}}$						
$k_{\ddot{\psi}}$	0.4357	–						

after approximately 10 rotations around the yaw axis, which was discovered by software in the loop simulations. As a temporary solution for this problem, the gain of the angle correction was reduced about a factor of 100 in case the norm of the attitude error gets above a predefined threshold[5]. This change allows the unmodified EKF to be used in normal operation, but automatic scheduling of the gain provides stable operation during fast, sustained rotations. The motor speed controller (ESC) runs the BLHeli_32 Rev32.7 firmware.

[5]See Git commit 0cff682f in the final source code for flight test.

Except where otherwise noted, content of this paper is licensed under a Creative Commons Attribution 4.0 International License.

The reproduction and distribution with attribution of the entire paper or of individual pages, in electronic or printed form, including some materials under non-CC-BY 4.0 licenses is hereby granted by the respective copyright owners.

4.2 Simulation

The simulation is carried out in Matlab/Simulink using the Heun integration method at 1200 Hz to compute the flight dynamics. No sensor models or state estimations are included so that the controller measurement input is the undisturbed output of the flight dynamics module.

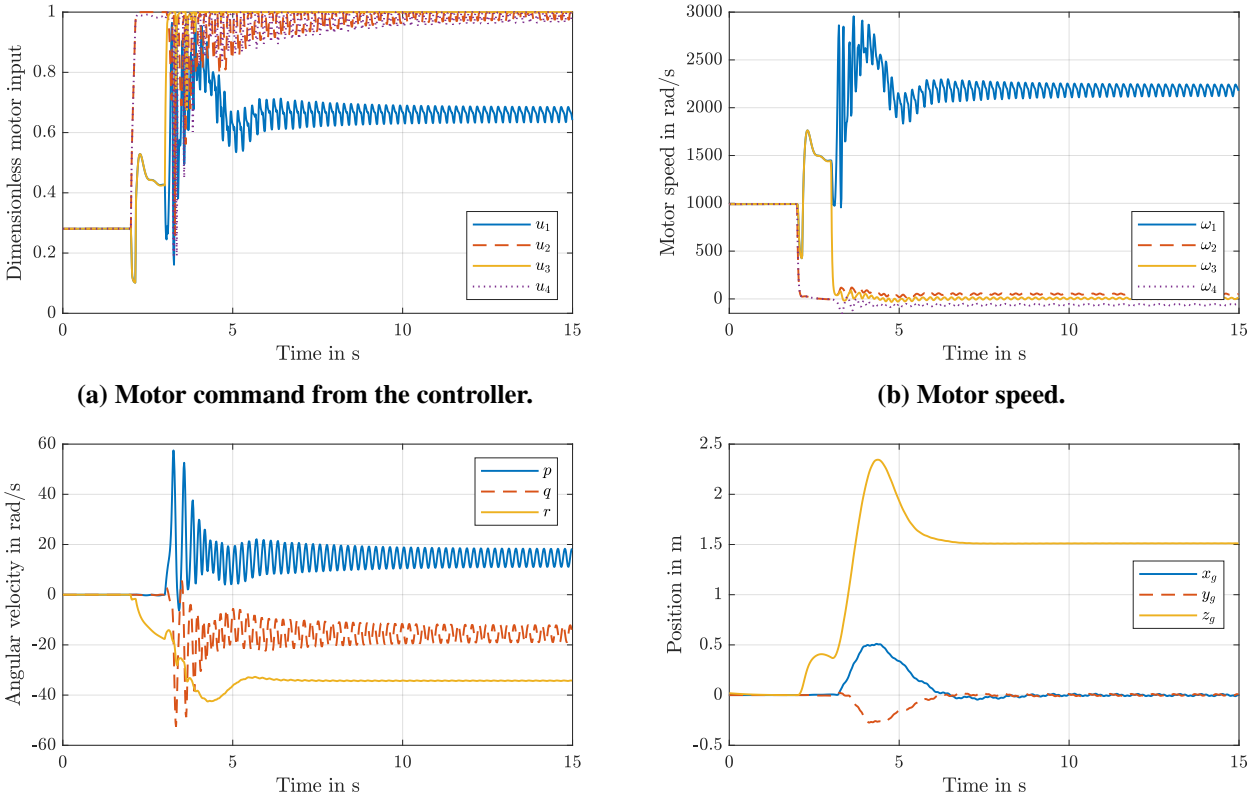

(a) Motor command from the controller.

(b) Motor speed.

(c) Angular rates in body frame.

(d) Position in the inertial frame.

Fig. 7 Simulation of successive rotor failures. Motor 2 and 4 are switched off after 1 s. Motor 3 fails one second later. A moderate rotational damping of $\Gamma = 0.0019\,\mathrm{Nm/(rad/s)}$ is used.

A simultaneous shutdown of the opposing motors 2 and 4 and subsequent shutdown of motor 3 is shown in Fig. 7. The fault error is induced in hover after one second and leads to hardly noticeable position errors, which is consistent with the results from other studies. Here, the remaining motors accelerate jerkily after a short delay and a yaw rate builds up. The controller, which has not received any direct info about the rotor failures, sends a maximum power request to the affected motors in a very short time after the failures. The remaining motors are controlled with a reduced power demand in the very short time until the maximum power demand of the other motors has built up. By looking at the commanded power requirements in this way, the passive fault-tolerant operation of this control scheme can be explained. As soon as a motor command reaches the maximum value, the CA algorithm starts to prioritize the required roll and pitch accelerations over the required yaw acceleration according to its parameterization. This automatically builds up and achieves the yaw rate required for stabilization.

The third motor is switched off one second after the first two motors. At this point, the quadrotor has already been set into rapid rotation around the yaw axis. The reactions of flight controller and quadrotor now strongly depend on the parameterization of the CA algorithm. If the required vertical acceleration is not strongly prioritized over the roll and pitch acceleration, the quadrotor will lose a lot of altitude. This is because the quadrotor must inevitably have built up a pitch and roll angle at the stable dynamic operating point with only one active motor (which can be seen from the permanent rotation rates about the roll and pitch axes). With the control concept used here, this means that a permanent control error in the pitch and roll angle must be tolerated. However, during normal operation of the quadrotor, prioritizing

Except where otherwise noted, content of this paper is licensed under a Creative Commons Attribution 4.0 International License.

The reproduction and distribution with attribution of the entire paper or of individual pages, in electronic or printed form, including some materials under non-CC-BY 4.0 licenses is hereby granted by the respective copyright owners.

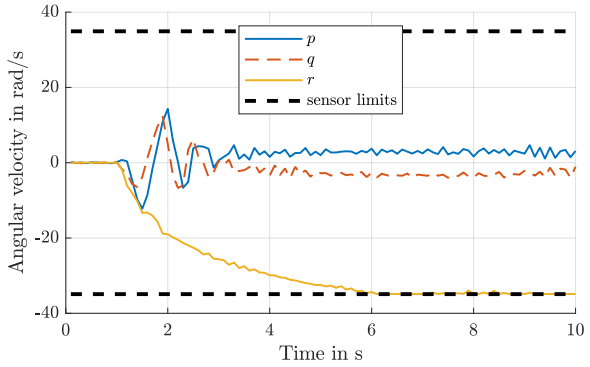

(a) Angular rates in body frame without cardboard.

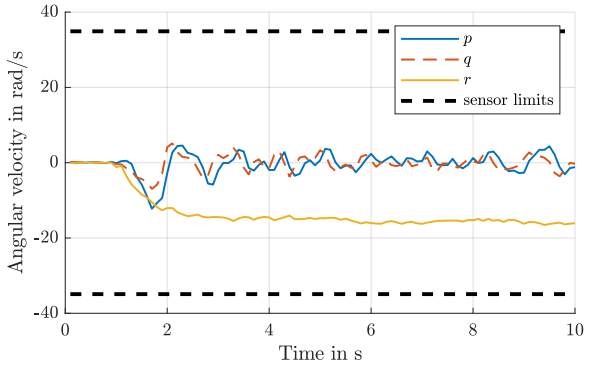

(b) Angular rates in body frame with cardboard.

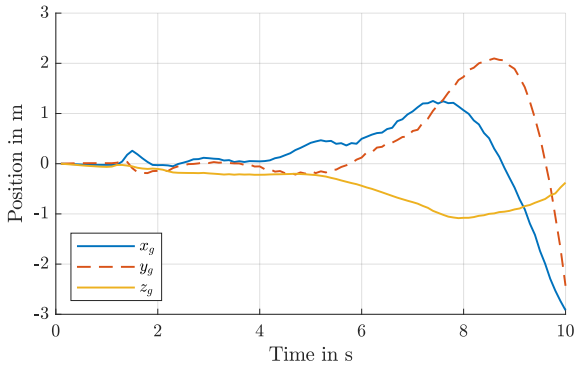

(c) Position in the inertial frame without cardboard.

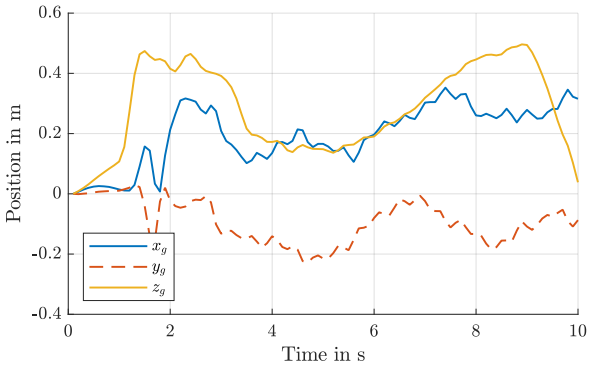

(d) Position in the inertial frame with cardboard.

Fig. 8 Two flight tests with two opposing rotor failures, left without cardboard, right with cardboard. Motor 2 and 4 are switched off after 1 s and the quadrotor remains stable. Without the cardboard the gyro measuring the yaw rate saturates after 6 s at 2000 degrees/s and the quadrotor loses control.

the required vertical acceleration over roll and pitch acceleration may be undesirable [15]. As a simple proposed solution, we have therefore automatically adjusted the weighting of the vertical acceleration in the CA algorithm from the rotation speed around the thrust vector:

$$\Delta w_{\ddot{z}} = \frac{\Delta w_{\ddot{z},\max}}{2}\left(1+\tanh\left(\frac{2.297}{r_{\text{range}}}\frac{\text{s}}{\text{rad}}\cdot\left(\frac{|\boldsymbol{n}\cdot\boldsymbol{\Omega}|}{\|\boldsymbol{\Omega}\|}\cdot|r_{\text{f}}|-r_{\text{mid}}\right)\right)\right). \tag{28}$$

Satisfactory results were achieved with $\Delta w_{\ddot{z},\max} = 300\,\text{s}^2/\text{m}$, $r_{\text{mid}} = 8\,\text{rad/s}$ and $r_{\text{range}} = 6\,\text{rad/s}$. From Eq. (28) follows $0 \leq \Delta w_{\ddot{z}} \leq \Delta w_{\ddot{z},\max}$ and $\Delta w_{\ddot{z}} = \Delta w_{\ddot{z},\max}/2$ if $|r_{\text{f}}| = r_{\text{mid}}$ and if $|\boldsymbol{n}\cdot\boldsymbol{\Omega}|/\|\boldsymbol{\Omega}\| = 1$ (angular velocity vector is parallel to the thrust vector). Moreover, $\Delta w_{\ddot{z}} = 1\,\% \cdot \Delta w_{\ddot{z},\max}$ if $|r_{\text{f}}| = r_{\text{mid}} - r_{\text{range}}$ and if $|\boldsymbol{n}\cdot\boldsymbol{\Omega}|/\|\boldsymbol{\Omega}\| = 1$. The remaining altitude error, see Fig. 7d, depends on the weighting between the required vertical acceleration and the roll and pitch acceleration in the CA algorithm.

Based on the previous explanations, we assume that a simultaneous failure of three motors cannot generally be compensated with this control concept. If all motors fail at the same time, the remaining motor generates torque mainly by its thrust and not by its drag. Thus, the controllable torque hardly acts in the desired direction to make the quadrotor rotate around its thrust vector. Instead, the quadrotor is set in rotation mainly around its pitch or roll axis, initially getting into a state that is generally undesirable. From this state, the controller was unable to transition the quadrotor to the desired stable dynamic operating point in our studies. We are also not aware of any study that calculates the optimal trajectory in the presence of a simultaneous triple rotor failure. Therefore, it is also not known which position errors are to be expected at least in the event of such a failure. The strong oscillations in Fig. 7 can be decreased by switching off the third motor smoothly.

Except where otherwise noted, content of this paper is licensed under a Creative Commons Attribution 4.0 International License.

The reproduction and distribution with attribution of the entire paper or of individual pages, in electronic or printed form, including some materials under non-CC-BY 4.0 licenses is hereby granted by the respective copyright owners.

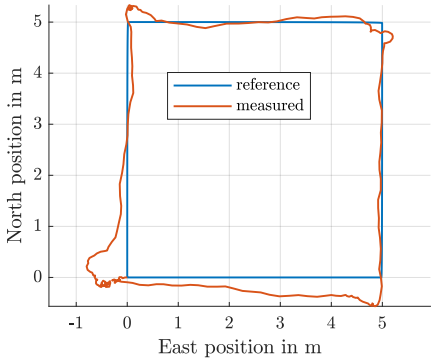

(a) Flight test with cardboard.

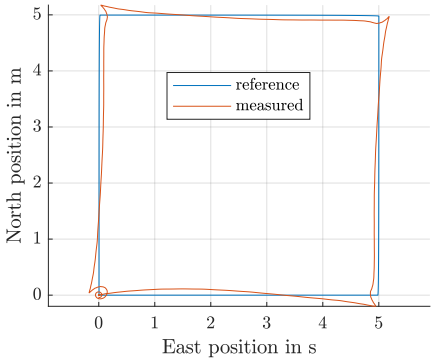

(b) Simulation with equal rotational damping.

Fig. 9 Position control with two opposing rotor failures. At each corner, the target speed is zero and a total of 5 seconds is required for each edge. Start and end at zero, counterclockwise flight direction.

4.3 Flight Test

During the first flight tests, the controller was able to stabilize the quadrotor as expected when two motors abruptly shut down. However, the yaw damping of the quadrotor in the flight test was lower than assumed in the simulation, causing the quadrotor to reach an unmeasurable yaw rate of 2000 °/s a few seconds after the motors were switched off, see Fig. 8a. The results of such a flight test are shown in Fig. 8 in the left column. When the limit rate of any gyro is reached, the EKF and the controller become unstable and the quadrotor crashes a few seconds later.

That is why the yaw damping was increased artificially by means of cardboard attached to the motor arms, see Fig. 6b. The right column of Fig. 8 shows the same failure but a significantly lower yaw rate, see Fig. 8b. Compared to simulation results, see Fig. 7, the vertical position error was limited to approximately 0.5 m. However, moderate lateral position errors also occur due to wind, among other factors. A third rotor failure has not yet been successfully flight tested.

Figure 9 demonstrates the tracking performance in the case of two opposing rotor failures. Overall, the tracking performance is satisfactory with position errors in the decimeter range in the case of the ideal simulation and position errors in the range of half a meter in the case of the flight test.

5 Conclusion

In this paper, a passive FTC based on INDI and CA is developed for a quadrotor. As expected, the controller proves to be very robust and, thanks to the CA, can compensate for a single and two opposite rotor failures with only minor short-term position errors. A third rotor failure can only be compensated under certain conditions: The quadrotor must have been previously started spinning around an average thrust direction and the weighting of the desired vertical acceleration in the CA algorithm must be significantly higher than the weighting of the desired roll and pitch acceleration. However, the compensation of two adjacent rotor failures cannot be compensated by this passive FTC. We also demonstrate that rotor failures can be compensated outdoors. For this purpose, a standard state estimator (Extended Kalman Filter) was slightly modified to provide a stable solution even in the presence of fast permanent rotation.

In the future, a third motor failure should be demonstrated in flight tests. Moreover, the performance of this passive FTC should be compared with active FTC. In addition, the transition could be calculated for three rotor failures with nonlinear optimal control as a benchmark.

Except where otherwise noted, content of this paper is licensed under a Creative Commons Attribution 4.0 International License.

The reproduction and distribution with attribution of the entire paper or of individual pages, in electronic or printed form, including some materials under non-CC-BY 4.0 licenses is hereby granted by the respective copyright owners.

Appendix

Table 3 Components of the quadrotor Minnie

Component	Label
Motors	Brotherhobby VY 2004 Motor 1700KV
Battery	Tattu R-Line 4.0 6s 1300mAh 130C Lipo
ESC	Holybro Tekko32 F3 4in1 40A ESC
Propellers	Gemfan 5125 SL Hurricane 5.1” 3-Blade
Frame	aMAXinno F6Mini 6”
Flight controller board	Matek H743-SLIM

Acknowledgments

We would like to acknowledge the funding of the methods of flight control development by the Deutsche Forschungsgemeinschaft (DFG, German Research Foundation) under Germany’s Excellence Strategy – EXC 2163/1 - Sustainable and Energy Efficient Aviation – Project-ID 390881007. Furthermore, we thank Josias Cierpka (TU Braunschweig, AKAMAV) for his support setting up the ArduCopter interface and Jonas Withelm (TU Braunschweig, AKAMAV) for his support setting up the quadrotor Minnie.

References

[1] Alessandro Freddi, Alexander Lanzon, and Sauro Longhi. A feedback linearization approach to fault tolerance in quadrotor vehicles. *IFAC proceedings volumes*, 44(1):5413–5418, 2011. DOI: 10.3182/20110828-6-IT-1002.02016.

[2] Mark W Mueller and Raffaello D’Andrea. Stability and control of a quadrocopter despite the complete loss of one, two, or three propellers. In *2014 IEEE international conference on robotics and automation (ICRA)*, pages 45–52. IEEE, 2014. DOI: 10.1109/ICRA.2014.6906588.

[3] Alexander Lanzon, Alessandro Freddi, and Sauro Longhi. Flight control of a quadrotor vehicle subsequent to a rotor failure. *Journal of Guidance, Control, and Dynamics*, 37(2):580–591, 2014. DOI: 10.2514/1.59869.

[4] Mark W Mueller and Raffaello D’Andrea. Relaxed hover solutions for multicopters: Application to algorithmic redundancy and novel vehicles. *The International Journal of Robotics Research*, 35(8):873–889, 2016. DOI: 10.1177/0278364915596233.

[5] Yury V Morozov. Emergency control of a quadrocopter in case of failure of two symmetric propellers. *Autom. Remote. Control.*, 79(3):463–478, 2018. DOI: 10.1134/S0005117918030062.

[6] Vincenzo Lippiello, Fabio Ruggiero, and Diana Serra. Emergency landing for a quadrotor in case of a propeller failure: A PID based approach. In *2014 IEEE International Symposium on Safety, Security, and Rescue Robotics (2014)*, pages 1–7. IEEE, 2014. DOI: 10.1109/SSRR.2014.7017647.

[7] Johannes Stephan, Lorenz Schmitt, and Walter Fichter. Linear parameter-varying control for quadrotors in case of complete actuator loss. *Journal of Guidance, Control, and Dynamics*, 41(10):2232–2246, 2018. DOI: 10.2514/1.G003441.

Except where otherwise noted, content of this paper is licensed under a Creative Commons Attribution 4.0 International License.

The reproduction and distribution with attribution of the entire paper or of individual pages, in electronic or printed form, including some materials under non-CC-BY 4.0 licenses is hereby granted by the respective copyright owners.

[8] S. Sun, G. Cioffi, C. de Visser, and D. Scaramuzza. Autonomous quadrotor flight despite rotor failure with onboard vision sensors: Frames vs. events. *IEEE Robotics and Automation Letters*, 6(2):580–587, 2021. DOI: 10.1109/LRA.2020.3048875.

[9] Vincenzo Lippiello, Fabio Ruggiero, and Diana Serra. Emergency landing for a quadrotor in case of a propeller failure: A backstepping approach. In *2014 IEEE/RSJ International Conference on Intelligent Robots and Systems*, pages 4782–4788. IEEE, 2014. DOI: 10.1109/IROS.2014.6943242.

[10] Peng Lu and Erik-Jan van Kampen. Active fault-tolerant control for quadrotors subjected to a complete rotor failure. In *2015 IEEE/RSJ International Conference on Intelligent Robots and Systems (IROS)*, pages 4698–4703. IEEE, 2015. DOI: 10.1109/IROS.2015.7354046.

[11] Sihao Sun, Leon Sijbers, Xuerui Wang, and Coen de Visser. High-speed flight of quadrotor despite loss of single rotor. *IEEE Robotics and Automation Letters*, 3(4):3201–3207, 2018. DOI: 10.1109/LRA.2018.2851028.

[12] Sihao Sun, Xuerui Wang, Qiping Chu, and Coen de Visser. Incremental nonlinear fault-tolerant control of a quadrotor with complete loss of two opposing rotors. *IEEE Transactions on Robotics*, 37(1):116–130, 2020. DOI: 10.1109/TRO.2020.3010626.

[13] Fang Nan, Sihao Sun, Philipp Foehn, and Davide Scaramuzza. Nonlinear MPC for quadrotor fault-tolerant control. *arXiv preprint arXiv:2109.12886*, 2021. DOI: 10.48550/arXiv.2109.12886.

[14] Sihao Sun, Matthias Baert, Bram Strack Van Schijndel, and Coen De Visser. Upset recovery control for quadrotors subjected to a complete rotor failure from large initial disturbances. In *2020 IEEE International Conference on Robotics and Automation (ICRA)*, pages 4273–4279. IEEE, 2020. DOI: 10.1109/ICRA40945.2020.9197239.

[15] Ewoud Smeur, Daan Höppener, and Christophe De Wagter. Prioritized control allocation for quadrotors subject to saturation. In *International Micro Air Vehicle Conference and Flight Competition*, number September, pages 37–43, 2017.

[16] Brian L Stevens, Frank L Lewis, and Eric N Johnson. *Aircraft control and simulation: dynamics, controls design, and autonomous systems*. John Wiley & Sons, 2015. DOI: 10.1002/9781119174882.

[17] Samir Bouabdallah, Andre Noth, and Roland Siegwart. PID vs LQ control techniques applied to an indoor micro quadrotor. In *2004 IEEE/RSJ International Conference on Intelligent Robots and Systems (IROS)(IEEE Cat. No. 04CH37566)*, volume 3, pages 2451–2456. IEEE, 2004. DOI: 10.1109/IROS.2004.1389776.

[18] Ewoud JJ Smeur, Guido CHE de Croon, and Qiping Chu. Cascaded incremental nonlinear dynamic inversion for mav disturbance rejection. *Control Engineering Practice*, 73:79–90, 2018. DOI: 10.1016/j.conengprac.2018.01.003.

[19] Ewoud JJ Smeur, Qiping Chu, and Guido CHE de Croon. Adaptive incremental nonlinear dynamic inversion for attitude control of micro air vehicles. *Journal of Guidance, Control, and Dynamics*, 39(3):450–461, 2016. DOI: 10.2514/1.G001490.

[20] Barton J Bacon, Aaron J Ostroff, and Suresh M Joshi. Reconfigurable NDI controller using inertial sensor failure detection & isolation. *IEEE Transactions on Aerospace and Electronic Systems*, 37(4):1373–1383, 2001. DOI: 10.1109/7.976972.

[21] Ola Harkegard. Efficient active set algorithms for solving constrained least squares problems in aircraft control allocation. In *Proceedings of the 41st IEEE Conference on Decision and Control, 2002.*, volume 2, pages 1295–1300. IEEE, 2002. DOI: 10.1109/CDC.2002.1184694.

Except where otherwise noted, content of this paper is licensed under a Creative Commons Attribution 4.0 International License.

The reproduction and distribution with attribution of the entire paper or of individual pages, in electronic or printed form, including some materials under non-CC-BY 4.0 licenses is hereby granted by the respective copyright owners.